Rock and Soil Mechanics

Volume 43 | Issue 1 Article 5

3-23-2022

Plastic deformation and hardening characteristics of the staggered zone under high in-situ stress unloading conditions

Shu-qian DUAN
State Key Laboratory of Geomechanics and Geotechnical Engineering, Institute of Rock and Soil Mechanics, Chinese Academy of Sciences, Wuhan, Hubei 430071, China

Po GAO
School of Civil Engineering, Zhengzhou University, Zhengzhou, Henan 450001, China

Quan JIANG
State Key Laboratory of Geomechanics and Geotechnical Engineering, Institute of Rock and Soil Mechanics, Chinese Academy of Sciences, Wuhan, Hubei 430071, China, qjiang@whrsm.ac.cn

Yang-yi ZHOU
Key Laboratory of Ministry of Education on Safe Mining of Deep Metal Mines, Northeastern University, Shenyang, Liaoning 110819, China

See next page for additional authors

Custom Citation

DUAN Shu-qian, GAO Po, JIANG Quan, ZHOU Yang-yi, XU Ding-ping, . Plastic deformation and hardening characteristics of the staggered zone under high in-situ stress unloading conditions[J]. Rock and Soil Mechanics, 2022, 43(1): 97-109.

Plastic deformation and hardening characteristics of the staggered zone under high in-situ stress unloading conditions

Authors

Shu-qian DUAN, Po GAO, Quan JIANG, Yang-yi ZHOU, and Ding-ping XU

Rock and Soil Mechanics 2022 43(1): 97−109 ISSN 1000−7598
https: //doi.org/10.16285/j.rsm.2021.5612 rocksoilmech.researchcommons.org/journal

Plastic deformation and hardening characteristics of the staggered zone under high in-situ stress unloading conditions

DUAN Shu-qian[1, 2], GAO Po[1], JIANG Quan[2], ZHOU Yang-yi[3], XU Ding-ping[2]

1. School of Civil Engineering, Zhengzhou University, Zhengzhou, Henan 450001, China

2. State Key Laboratory of Geomechanics and Geotechnical Engineering, Institute of Rock and Soil Mechanics, Chinese Academy of Sciences, Wuhan, Hubei 430071, China

3. Key Laboratory of Ministry of Education on Safe Mining of Deep Metal Mines, Northeastern University, Shenyang, Liaoning 110819, China

Abstract: To clarify the plastic law and hardening characteristics of deformation and failure of staggered zone under high in-situ stress unloading conditions with excavation in underground engineering, a series of triaxial tests under different confining pressures and different loading and unloading stress paths was conducted. The plastic deformation laws of the staggered zone under different loading and unloading stress paths were deeply investigated. Based on the results of the experiments, the dependency of stress path of internal variables such as the equivalent plastic work, the equivalent plastic strain and the plastic volumetric strain as hardening parameters were further explored in the stress space. Meanwhile, a modified formula for hardening parameters with the independency of stress path was proposed. The results showed that, 1) The effect of stress path was significant on the deformation properties of staggered zone under high in-situ stress. The high initial confining pressure would inhibit the development of the circumferential plastic deformation of samples with the staggered zone under the same unloading stress path. And the plastic volumetric residual strain (6%) of samples with the staggered zone under the stress path of unloading axial pressure and confining pressure was significantly greater than that of other unloading stress paths (2%−4%) under the same initial confining pressure. The promoting effects of different stress paths on the plastic volumetric deformation of the staggered zone were as follows. The promoting effect of the stress path of unloading axial pressure and unloading confining pressure was the strongest, that of the stress path of constant axial pressure and unloading confining pressure was the second stronger, and that of the stress path of loading axial pressure and unloading confining pressure was the weakest. 2) There were a certain of the dependency of stress path of its internal variables such as plastic volumetric strain, equivalent plastic strain and equivalent plastic work during the deformation and failure process of the staggered zone in different unloading stress paths. Therefore, it is not accurate to directly take any of the above state parameters as the hardening parameters and assume that it is independent of the stress paths in the elastic-plastic analysis of staggered zone. Therefore, a modified method of the equivalent plastic work was proposed. It was found that when the parameter n_s reflecting the material properties of staggered zone was equal to −0.4, the modified equivalent plastic work had the obvious independency of stress path, which was more appropriate for describing the unloading plastic strain hardening characteristics of the staggered zone under high in-situ stress unloading conditions. The plastic mechanical characteristics of the staggered zone revealed in this paper can further deepen the understanding of deformation and failure of the staggered zone under high in-situ stress unloading conditions, and provide a theoretical basis for the analysis of the failure mechanism and support control of the staggered zone in practical engineering.

Keywords: staggered zone; high in-situ stress; unloading; plastic deformation; hardening characteristics

1 Introduction

Since the 21st century, in order to build a world-class clean energy corridor, China has planned and built a number of large-scale hydropower development energy bases in the southwest region, which is rich in water resources. These hydropower development energy bases are mostly concentrated in the high mountains and valleys of the west, where the physical, chemical and mechanical environments are special and complex, and the geological environment is fragile. Their construction scale and technical difficulty are unprecedented[1]. Especially, when it encounters a large geological structural staggered zone, its mechanical response becomes more complex under the disturbed stress path of high in-situ stress due to the various spatial topological relationships between the high ductility and high risk of the staggered zone and the free surface with complex excavation (see Fig. 1). The rock mass near the staggered zone will suffer from engineering failure with different scales and degrees,

Received: 21 April 2021 Revised: 22 September 2021
This work was supported by the National Natural Science Foundation of China (51909241), the Scientific Research Key Project Fund of Colleges and Universities of Henan Province (19A560006) and the Open Research Fund of State Key Laboratory of Geomechanics and Geotechnical Engineering, Institute of Rock and Soil Mechanics, Chinese Academy of Sciences (Z017011).
First author: DUAN Shu-qian, female, born in 1991, PhD, Associate Professor, mainly engaged in research on rock mechanics and engineering. E-mail: shuqianduan@zzu.edu.cn
Corresponding author: JIANG Quan, male, born in 1978, PhD, Professor, mainly engaged in research on rock mechanics and underground engineering. E-mail: qjiang@whrsm.ac.cn

such as the plastic extrusion tensile failure and structural collapse failure with stress type, as well as the support failure in anchor bolts and anchor cables[2−6], which seriously affect the stability of underground caverns and should attach great importance. Therefore, it is significant to study the deformation, failure mechanism and mechanical properties of the staggered zone for the stability analysis of the staggered zone itself and the rock mass containing the staggered zone during the construction process of deep underground engineering.

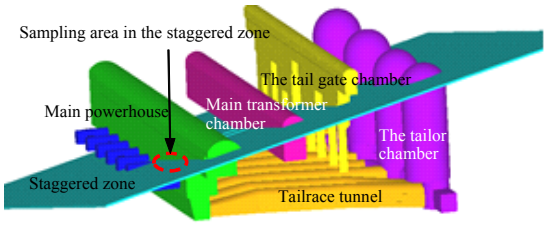

(a) Spatial distribution of deep underground caverns and staggered zone

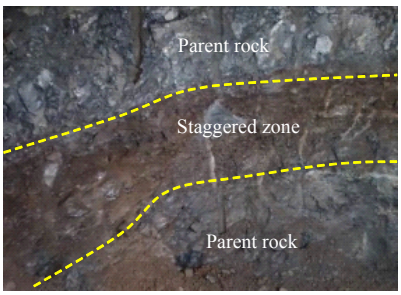

(b) The field disclosure form of the staggered zone

Fig. 1 Spatial distribution of buried underground caverns and staggered zone in southwestern, China

Existing studies on loading and unloading mechanical properties and failure characteristics of the staggered zone show that its mechanical response is obviously synergistically affected and controlled by high in-situ stress level and complex unloading stress path[3]. Meanwhile, the failure mode of the staggered zone is also closely related to the loading and unloading stress path. Among them, the samples from the staggered zone all show the "waist drum" failure mode under the conventional triaxial loading and unloading condition. Additionally, compared with the conventional triaxial loading test, the samples from the staggered zone under the unloading stress path show the deformation characteristics of strong unloading rebound, dilatancy and plastic hardening. Meanwhile, the tensile/tensile−shear cracks both appear on the surface of the samples from the staggered zone, and the samples from the staggered zone enter the failure state just need a shorter time[7]. The plastic strain, a part of the total strain, begins to play an important role when the staggered zone reaches the elastic deformation limit. In the yield and failure stages under different stress paths, the change and development of plastic strain will affect the deformation development and failure mode of rocks and soil[8−10]. Currently, there is no comprehensive theory about the dependence of plastic deformation on stress path, especially the plastic deformation law of the staggered zone under high in-situ stress unloading condition is nor relevant research report.

After plastic deformation occurs in the staggered zone under the high in-situ stress unloading condition, the yield condition will change and the yield stress will change with it. Scholars[3, 11] called the yield condition that changes with the development of plastic deformation as the hardening condition. To describe the hardening condition, a characteristic internal variable describing the change of loading surface independent of stress path, namely hardening parameter, should be introduced[11]. Meanwhile, to find internal variables that conform to the definition of hardening parameters, many different expressions of hardening parameters have been proposed based on relatively simple stress path tests, among which the most common ones are the plastic volumetric strain, equivalent plastic strain and equivalent plastic work[12]. Fumio [13] proposed the assumption that the plastic shear strain was used as the hardening parameter, and proved its rationality as hardening parameter of Japanese Toyoura sand through a series of numerical analysis. Huang et al.[14−15] proposed the research idea that plastic potential surface, yield surface and hardening parameters which can be directly determined by tests. Yao et al.[16−18] conducted a series of simple triaxial tensile and triaxial compression tests, and further discussed the dependency of stress path of hardening parameters such as plastic shear strain, plastic volumetric strain, plastic work, hardening parameters of Tsinghua model and unified hardening parameter H. For rocks and soil materials with special physical and mechanical properties, Ma et al.[19−20] modified hardening parameters such as plastic work, to better describe the hardening law of rocks and soil materials. However, some experimental results[21−24] show that the stress path constructed relying on the above hardening parameters is relatively simple, and the differences of physical and mechanical properties of different rocks and soil materials are not fully considered. Therefore, these conventional hardening parameters are often not completely independent of the stress path, and it is difficult to extend them to the general geotechnical elastoplastic theory. Consequently, for different types of rocks and soil, especially for the special rocks and soil materials such as staggered zone, their hardening parameters under high in-situ stress and complex stress path need to be selected and modified.

In this paper, the staggered zone exposed during the excavation of a large underground powerhouse is taken as the research object, and its plastic deformation law is carefully analyzed and revealed considering

enough the complex historical conditions of high in-situ stress loading and unloading. Based on the test results, the characteristics included the plastic volumetric strain, equivalent plastic strain and equivalent plastic work both regarded as the hardening parameters of the dependency of stress path of the staggered zone were quantitative explored. Meanwhile, a modified hardening parameter with the independency of stress path under complex unloading stress path was proposed to describe the plastic deformation and hardening characteristics of the staggered zone under high unloading stress. The research could further enrich the understanding of the deformation and failure mechanism of staggered zone, and provide the theoretical support for prevention and control of staggered zone engineering.

2 Test equipment and procedures

2.1 Sample preparation

The samples from the staggered zone were taken from a large underground powerhouse located at a vertical buried depth of about 260−330 m and with a height of 88.7 m, of a hydropower station in southwest, China (see Fig. 1(a)). In the sampling area, the location where the thickness of the staggered zone is greater than 10 cm and about 40 cm away from the tunnel wall is selected as the sampling spot. As shown in Fig. 2(a), the sampling tool of the staggered zone [25] is used to insert into the sampling spot to obtain the samples of the staggered zone with the density and the water content tended to be consistent, to ensure that the original characteristics of the staggered zone are not disturbed to the maximum extent. The cylindrical samples will be sealed and fixed, and numbered, recorded, with a special vehicle back to the room. Considering the staggered zone was subjected to the confining pressure in the early geological history, the maximum principal stress measured near the sampling spot is 33.4 MPa. For the samples from the staggered zone delivered to the laboratory, a self-developed sampling device of the staggered zone[5] was used to make the samples be consolidated to the initial in-situ stress of 35 MPa. And then the standard cylindrical samples were made by referring to the "*Standard for soil test method*" (GB/T50123−1999)[26]. All samples after consolidation were tested by ultrasonic wave, and the samples with similar wave velocity and similar range of mean square error were selected as test samples to ensure that the discreteness of the samples in subsequent tests was within an acceptable range. The samples was sealed with plastic wrap and stored in greenhouse with a constant temperature (22 ℃) for testing. The sample preparation process was shown in Figs. 2(b)−2(d). Meanwhile, physical parameter test and mineral composition analysis test of X-ray diffraction were conducted. The uniformity coefficient, curvature coefficient, clay content and content of coarse grain of natural staggered zone were obtained by sieving method. The moisture content, natural density, void ratio, saturation and other related parameters of the natural staggered zone were obtained by drying method. The plastic limit and liquid limit of natural staggered zone were measured by liquid-plastic limit combine tester, and the plastic index was calculated. The typical physical and mechanical parameters and main mineral composition of the staggered zone obtained were shown in Tables 1− 2.

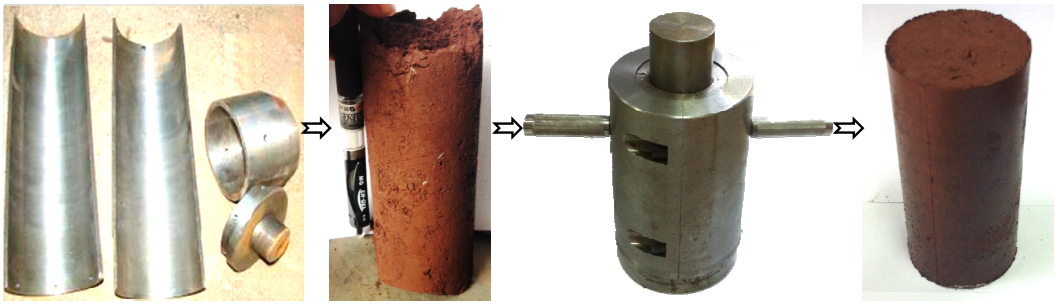

(a) Sampling tool with the open and close function [25] (b) Original-state samples obtained in field (c) Sampling tool for the staggered zone with the function of indoor open and close (d) Standard sample prepared

Fig. 2 Sample preparation reflecting the state of in-situ stress of staggered zone

Table 1 Geotechnical parameters of staggered zone

Geotechnical parameters	Calculation formulas/methods	Value	Geotechnical parameters	Calculation formulas/methods	Value
Uniformity coefficient C_u	$C_u = d_{60} / d_{10}$	100.91	Void ratio e	$e = V_v / V_s$	0.502
Curvature coefficient C_c	$C_c = d_{30}^2 / (d_{60} \times d_{10})$	2.57	Specific gravity G_S	$G_S = \rho \times g$	2.73
Clay content /%	$d < 0.005$ mm	8～15	Degree of saturation S_r /%	$S_r = V_w / V_v$	73
Content of coarse grain /%	$d > 2$ mm	25～35	Plastic limit W_P /%	Liquid-plastic limit	13.9
Moisture content /%	(m_s / m_d)	13.5	Liquid limit W_L /%	combine tester	24.7
Natural density ρ /(g • cm^{-3})	$\rho = m / V$	2.20	Plastic index I_P	$I_P = W_L - W_P$	10.8

Note: d_{60}, d_{30} and d_{10} represent the diameters of screen aperture corresponding to the passing of 60%, 30% and 10%, respectively; d is the particle size of the natural sample m, m_s and m_d are the mass of natural sample, the mass of water in natural sample and the mass of samples after drying; V, V_v, V_s and V_w are the volume of natural sample, the volume of void in natural sample, the volume of skeleton of natural samples and the volume of water in natural sample; g is the constant of gravity.

Table 2 Mineral composition of staggered zone

Mineral composition	Component proportion /%
Hematite	20
Montmorillonite	8
Ilmenite (I/S)	60
Sphene	12

2.2 Test equipment

The undrained triaxial loading and unloading tests of staggered zone were conducted by the advanced electro-hydraulic servo-controlled rock mechanics testing system (MTS815-04) (see Fig. 3), and the axial and circumferential deformation range met the deformation requirements of the stress path of the staggered zone.

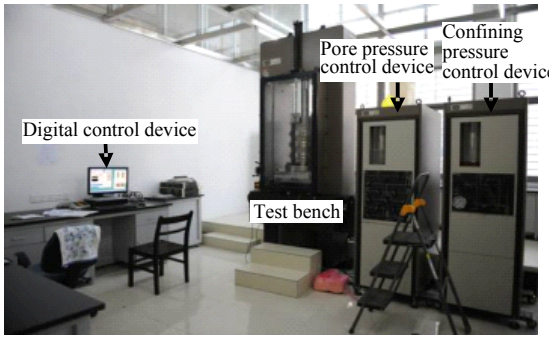

Fig. 3 MTS815-04 Electro-hydraulic servo-controlled rock mechanics testing system

2.3 Stress path

Field observation and numerical analysis of related staggered zone indicate [3, 27] that the processes of stress re-distribution of staggered zone are different when they are exposed at different positions of large underground caverns. When the staggered zone is exposed to the vault or shoulder, the most typical stress path is that the maximum principal stress σ_1 keeps constant or increases while the minimum principal stress σ_3 decreases (see the stress path Ⅱ or Ⅲ in Fig. 4). When the staggered zone is exposed at the high side wall of a large underground cavern, both the maximum principal stress σ_1 and the minimum principal stress σ_3 decrease (see the stress path Ⅳ in Fig. 4). Additionally, the stress path Ⅰ in Fig. 4 is a conventional triaxial loading stress path. And the deformation characteristics of the staggered zone under this stress path have been deeply studied in literature[3,7], the unloading stress path is more consistent with the in-situ stress re-distribution process, and is more likely to cause the failure of rocks from the staggered zone [4−5, 28−29]. Therefore, the focus of this study is the plastic deformation behavior of the staggered zone under the unloading stress path (see the stress path Ⅱ or Ⅲ or Ⅳ in Fig. 4).

2.4 Process of tests

To cover different stress states, the initial confining pressure σ_0 was designed as three stress levels of 5, 15 and 25 MPa in the test design of the stress path. Taking the triaxial test under stress path Ⅲ as an example, 0.5 kN external load can be pre-loaded to ensure a good contact between the indenter of the test instrument and the sample from the staggered zone before the formal test. Then, three principal stresses were set $\sigma_1=\sigma_2=\sigma_3$, which were simultaneously loaded to the pre-determined initial confining pressures (5, 15 and 25 MPa) with the loading rate of 0.05 MPa/s and stabilized for 5 min. Then, the axial shear rate with 0.005 mm/s increases σ_1 to 70% of the peak strength (the difference of maximum principal stress) of the sample from the staggered zone (corresponding to the turning point of volumetric strain). Finally, the maximum principal stress σ_1 keeps constant while the minimum principal stress σ_3 with the rate of 0.25 MPa/s decreases until the sample is damaged or reaches its limit displacement.

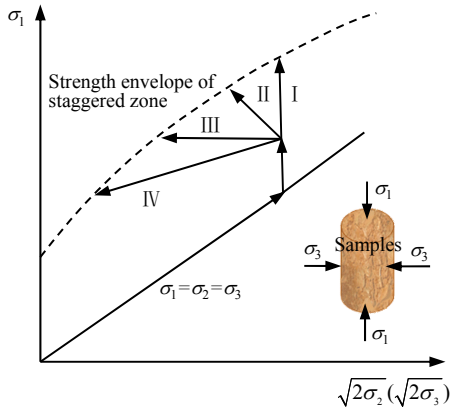

Fig. 4 Schematic diagram of stress paths in triaxial tests of staggered zone

The detailed process of sampling, sample preparation and triaxial test under different confining pressures and different stress paths was referred to the relevant instruments and test methods adopted by Duan et al. [7].

3 Experimental results and analysis

3.1 Overall deformation characteristics under unloading conditions

Figures 5(a) and 5(b) illustrate stress−strain curves and volumetric strain curves of the staggered zone under the same confining pressure (25 MPa) and different unloading stress paths. It can be seen that the staggered zone exhibits the strong plastic flow hardening characteristics and obvious dilatancy characteristics. Because there is no obvious peak stress point in the stress−strain curve, Duan et al. [7] divided the change curve of $\Delta\varepsilon_1/\Delta(\sigma_1-\sigma_3)$ and $\sigma_1-\sigma_3$ into two stages by incremental method. The deviatoric stress corresponding to the boundary point of stage ⅰ and stage ⅱ is defined as the ultimate bearing strength of

unloading σ_{qu}. Stage ii in Fig. 5(c) corresponds to the yield loading stage of the staggered zone, and there is an obvious turning point, which corresponds to the stable loading stage and unstable loading stage of the staggered zone before and after the turning point[30]. The deviatoric stress corresponding to the turning point can therefore be defined as the ultimate strength of unloading stable loading σ_{q+}.

Based on the above stress−strain curves, a typical full stress−strain curve was plotted for the staggered zone under unloading conditions, revealing the overall deformation characteristics of the staggered zone under high in-situ stresses and complex unloading conditions (see Fig. 5(d)). Stage *OA* in Fig. 5 (d) can be considered as the elastic stage with micro-cracks compaction and weak elastic deformation of samples, and point *A* corresponding the deviatoric stress is called the yield strength σ_s. As the load continues to increase, the plastic deformation such as the development of micro-cracks and the particle sliding together of sample, and stage *AB* shows the nonlinear relationship between the stress−strain curve. Starting from point *A*, the staggered zone begins to dilatancy, and the total volume deformation changes from compression to expansion near point *B*. After point *C*, with the gradual increase of deviatoric stress, the micro-cracks in the staggered zone further accumulate and converge, which makes its deformation increase sharply until a relatively complete failure surface is formed in the staggered zone and the failure occurs.

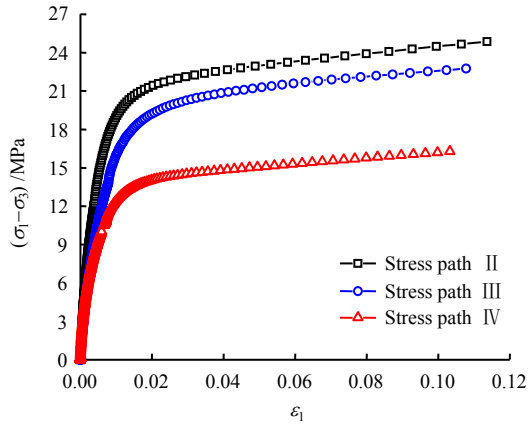

(a) Test stress−strain curves (25 MPa)

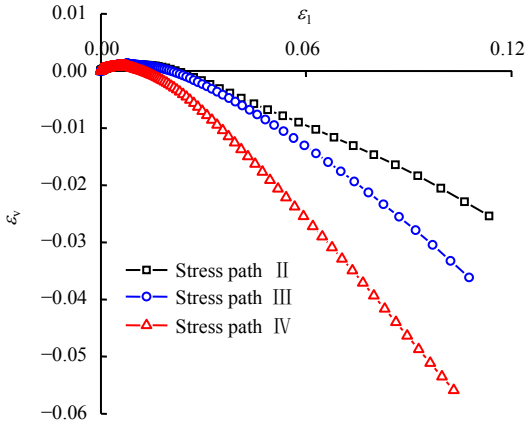

(b) Test volumetric strain−axial strain curves (25 MPa)

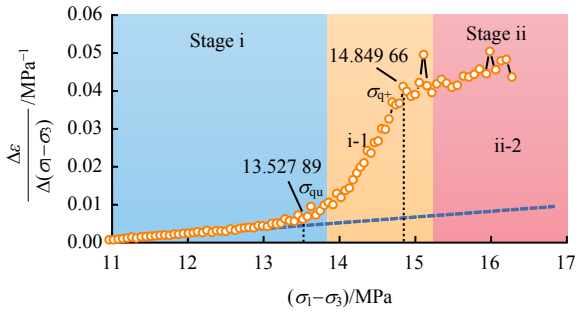

(c) Test curve of unloading ultimate bearing capacity (stress path Ⅳ at 25 MPa)

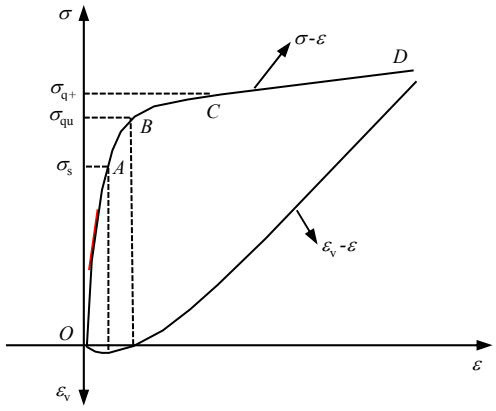

(d) Full stress−strain curves (refer to stress path Ⅳ at 25 MPa) [11]

Fig. 5 Typical stress-strain curves of samples from the staggered zone under unloading condition

3.2 Plastic deformation characteristics under unloading conditions

According to the analysis of Section 3.1, it is shown that the staggered zone has typical plastic hardening characteristics under the high in-situ stress unloading condition. After rock material enters to the plastic deformation, more attention should be paid to its plastic deformation, and its plastic strain can be observed and studied separately[31]. In this section, the plastic deformation characteristics of the staggered zone under complex high in-situ stress unloading path are deeply explored based on the existing research.

The staggered zone is a typical elasto-plastic geotechnical material, and its mechanical deformation can be divided into the elastic deformation and the plastic deformation, as is listed in Eq. (1):

$$\varepsilon_i = \varepsilon_i^{\mathrm{e}} + \varepsilon_i^{\mathrm{p}} \left(i = 1,3\right) \tag{1}$$

where ε_i, $\varepsilon_i^{\mathrm{e}}$ and $\varepsilon_i^{\mathrm{p}}$ are the elastic-plastic strain, elastic strain and plastic strain in direction *i*, respectively.

$$\left.\begin{aligned}\Delta\varepsilon_1 &= (\Delta\sigma_1 - 2\mu\Delta\sigma_3)/E \\ \Delta\varepsilon_3 &= [\Delta\sigma_3 - \mu(\Delta\sigma_1 + \Delta\sigma_3)]/E\end{aligned}\right\} \quad (2)$$

where $\Delta\sigma_1$ and $\Delta\sigma_3$ are the change differences of the first principal stress and the third principal stress, respectively; $\Delta\varepsilon_1$ and $\Delta\varepsilon_3$ are the change differences of the first principal strain and the third principal strain, respectively; μ is Poisson's ratio; and E is the elastic modulus (assuming E keeps constant during the confining pressure unloading).

Equation (2) is changed to obtain the elastic modulus E and Poisson's ratio μ:

$$E = (\Delta\sigma_1 - 2\mu\Delta\sigma_3)/\Delta\varepsilon_1 \quad (3)$$

$$\mu = \frac{\left(\Delta\sigma_3 - \dfrac{\Delta\varepsilon_3}{\Delta\varepsilon_1}\Delta\sigma_1\right)}{\left[\Delta\sigma_1 - \left(\dfrac{2\Delta\varepsilon_3}{\Delta\varepsilon_1} - 1\right)\Delta\sigma_3\right]} \quad (4)$$

According to the generalized Hooke's law, the elastic strain part of elastic-plastic deformation can be obtained as follows:

$$\varepsilon_1^{\mathrm{e}} = (\sigma_1 - 2\mu\sigma_3)/E \quad (5)$$

$$\varepsilon_3^{\mathrm{e}} = [\sigma_3 - \mu(\sigma_1 + \sigma_3)]/E \quad (6)$$

Considering that the staggered zone bears pressure difference for a long time under natural conditions, the elastic-plastic deformation of the loaded part has been completed before excavation with unloading[7]. Therefore, only the plastic deformation produced from unloading can be studied under the unloading stress path, and the deviatoric stress at the initial unloading point can be regarded as the initial yield strength of the staggered zone. The elastic modulus E and Poisson's ratio were re-calculated to ensure that the plastic strain at the initial unloading point was 0, and then the elastic or plastic strain during the unloading process was calculated by Eqs. (1), (5) and (6).

From the ratio of plastic strain (see Fig. 6) with unloading stress path of staggered zone, the ratio of unloading plastic strain and confining pressure of staggered zone (see Fig. 7) and typical stress−plastic strain curves of staggered zone (see Fig. 8), the following law can be obtained:

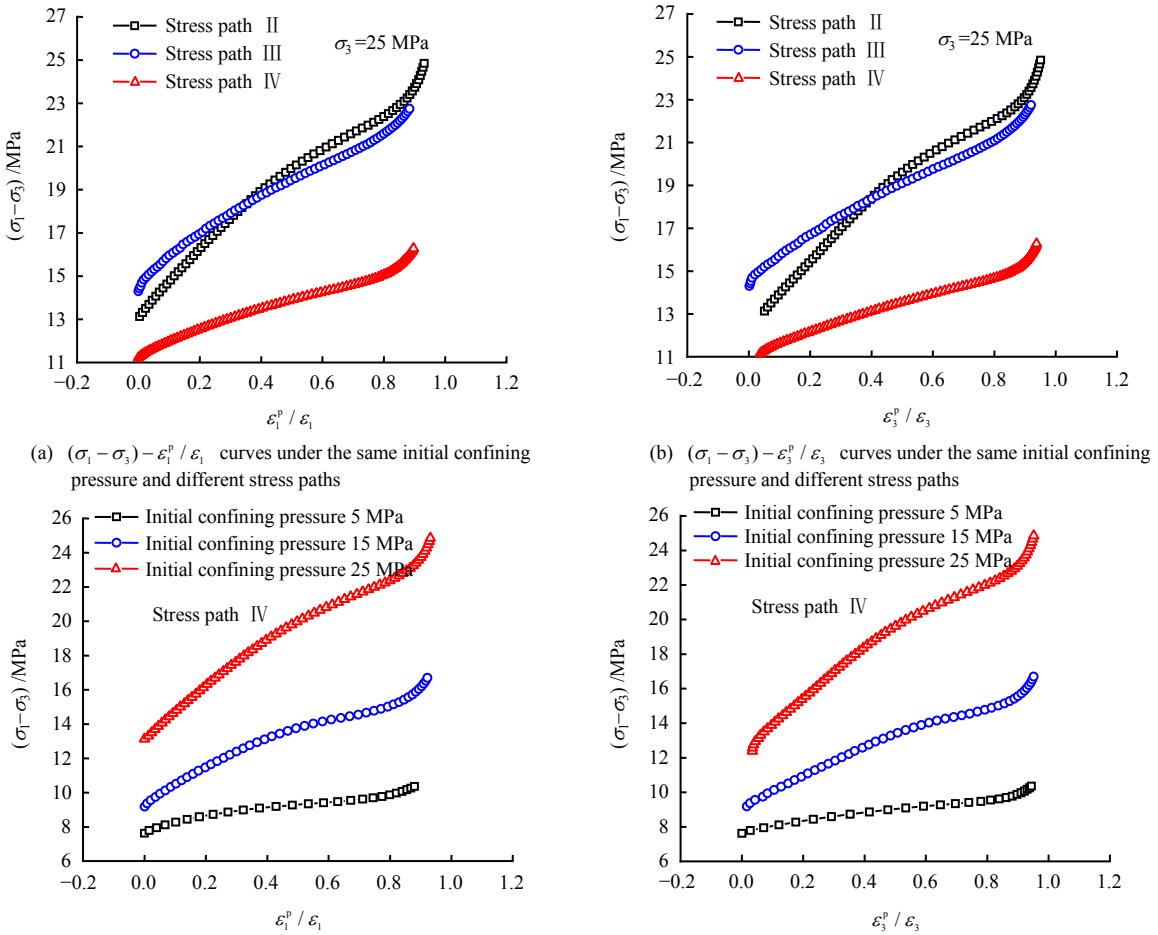

(a) $(\sigma_1 - \sigma_3) - \varepsilon_1^{\mathrm{p}}/\varepsilon_1$ curves under the same initial confining pressure and different stress paths

(b) $(\sigma_1 - \sigma_3) - \varepsilon_3^{\mathrm{p}}/\varepsilon_3$ curves under the same initial confining pressure and different stress paths

(c) $(\sigma_1 - \sigma_3) - \varepsilon_1^{\mathrm{p}}/\varepsilon_1$ curves under the same stress path and different initial confining pressures

(d) $(\sigma_1 - \sigma_3) - \varepsilon_3^{\mathrm{p}}/\varepsilon_3$ curves under the same stress path and different initial confining pressures

Fig. 6 The ratio of plastic strain of staggered zone under unloading stress path

(1) From the ratio of plastic strain after the initial unloading of the stagger zone under different stress paths and initial confining pressures (see Fig. 6), it could be observed that under the same initial confining

pressure (as shown in Figs. 6(a) and 6(b)), the stress path Ⅳ (unloading axial pressure and unloading confining pressure) had the strongest promoting effect on plastic deformation (the overall inclination of the curve was the most gentle), followed by the stress path Ⅲ (constant axial pressure and unloading confining pressure), and the stress path Ⅱ (increasing axial pressure and unloading confining pressure) was the weakest. When approaching the failure, the deformation of the staggered zone under each unloading stress path almost all come from the plastic deformation ($\varepsilon_i^{\mathrm{p}}/\varepsilon_i \approx 1$), and its change rate of plastic deformation slowed down. The ratio of plastic strain of the samples under the same stress path (stress path Ⅳ) and different initial confining pressures was analyzed (Figs. 6(c) and 6(d)). It could be seen that the higher the initial confining pressure was, the higher the slope of $(\sigma_1-\sigma_3)-\varepsilon_i^{\mathrm{p}}/\varepsilon_i$ was and the slower the growth of plastic deformation was. Namely, high confining pressure would inhibit the development of plastic deformation under the same stress path.

(2) The larger the ratio of plastic strain and confining pressure was, the more sensitive to the confining pressure unloading. The plastic volumetric strain in stress path Ⅳ was the most sensitive to confining pressure unloading and the plastic volumetric expansion was the most significant. The ratio of plastic volumetric strain and confining pressure and the plastic volumetric expansion in stress path Ⅱ were the smallest. However, stress path Ⅳ was the smallest while stress path Ⅱ was the largest from the perspective of ratio of axial unloading strain and confining pressure and the ratio of circumferential unloading strain and confining pressure (see Fig. 7). Additionally, it was considered that increasing axial pressure in stress path Ⅱ boosted the axial compression deformation more significantly than the circumferential expansion deformation. However, stress path Ⅳ was bidirectional unloading, that was, the staggered zone expanded outward in both axial and circumferential plastic deformation. Consequently, the volumetric plastic deformation was the most exquisite.

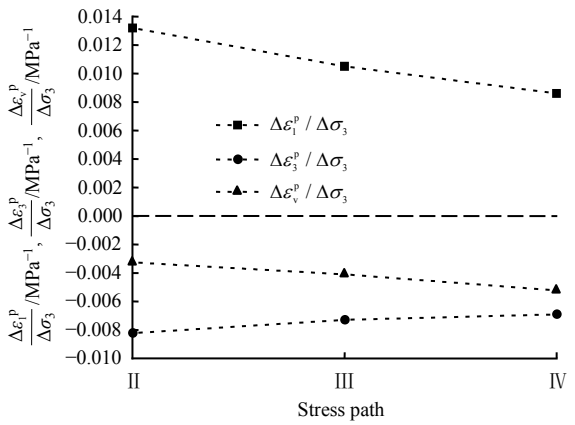

Fig. 7 The ratio of unloading plastic strain and confining pressure of staggered zone

(3) Starting from unloading point, the plastic volumetric strain of the staggered zone under each unloading stress path continued to reduce to zero, then the curve slope turned to left, and the plastic volumetric strain increased along the opposite direction. Approaching the turning point, the slope of axial plastic strain curve suddenly decreased, and the slope of circumferential plastic strain curve increased steadily. At the moment, the circumferential plastic deformation ($2\varepsilon_3^{\mathrm{p}}$) was more significant than the axial plastic deformation. Both axial and circumferential plastic deformations are greatly developed when approaching to the failure (see Fig. 8). Meanwhile, it could be seen that the change trend of plastic volumetric strain curve and the circumferential plastic strain curve were basically the same in the unloading test, namely, the law of plastic volumetric change mainly depended on the circumferential plastic strain. When the stress path was the same and the same circumferential plastic deformation was produced, the deviatoric stress increased with the increasing of the confining pressure. When the initial confining pressure was the same and the same circumferential plastic deformation was produced, the deviatoric stress corresponding to stress path Ⅳ was the smallest, followed by stress path Ⅲ, and stress path Ⅱ was the largest. Under the action of high confining pressure, the stress path Ⅳ showed a stress−plastic strain-hardening phenomenon. The plastic volumetric residual strain of stress path Ⅳ (6%) was significantly greater than that of the other stress paths (2%−4%), namely, the stress path Ⅳ (unloading axial pressure and unloading confining pressure) could best benefit the development of plastic volumetric strain most. The above analysis showed that increasing the confining pressure would inhibit the development of circumferential plastic strain. And the promoted effects of the same confining pressure (25 MPa) and different unloading stress paths on plastic deformation were different. Among them, the promoted effect of the stress path Ⅳ was strongest, that of the stress path Ⅲ was second stronger, and that of the stress path Ⅱ was the weakest.

4 Hardening characteristics of staggered zone

4.1 Dependency of stress path of basic hardening parameters

Most of the existing geo-static elastoplastic models were adopted with the isosurface hardening theory. To simplify the issue, it was assumed that the direction of principal stress did not change, the shape of the loading surface remains unchanged, and only the shape is enlarged (hardening) or reduced (softening) in the stress space, namely, the yield surface (loading surface) was regarded as the isosurface of a hardening parameter[11]. The selection of hardening parameters

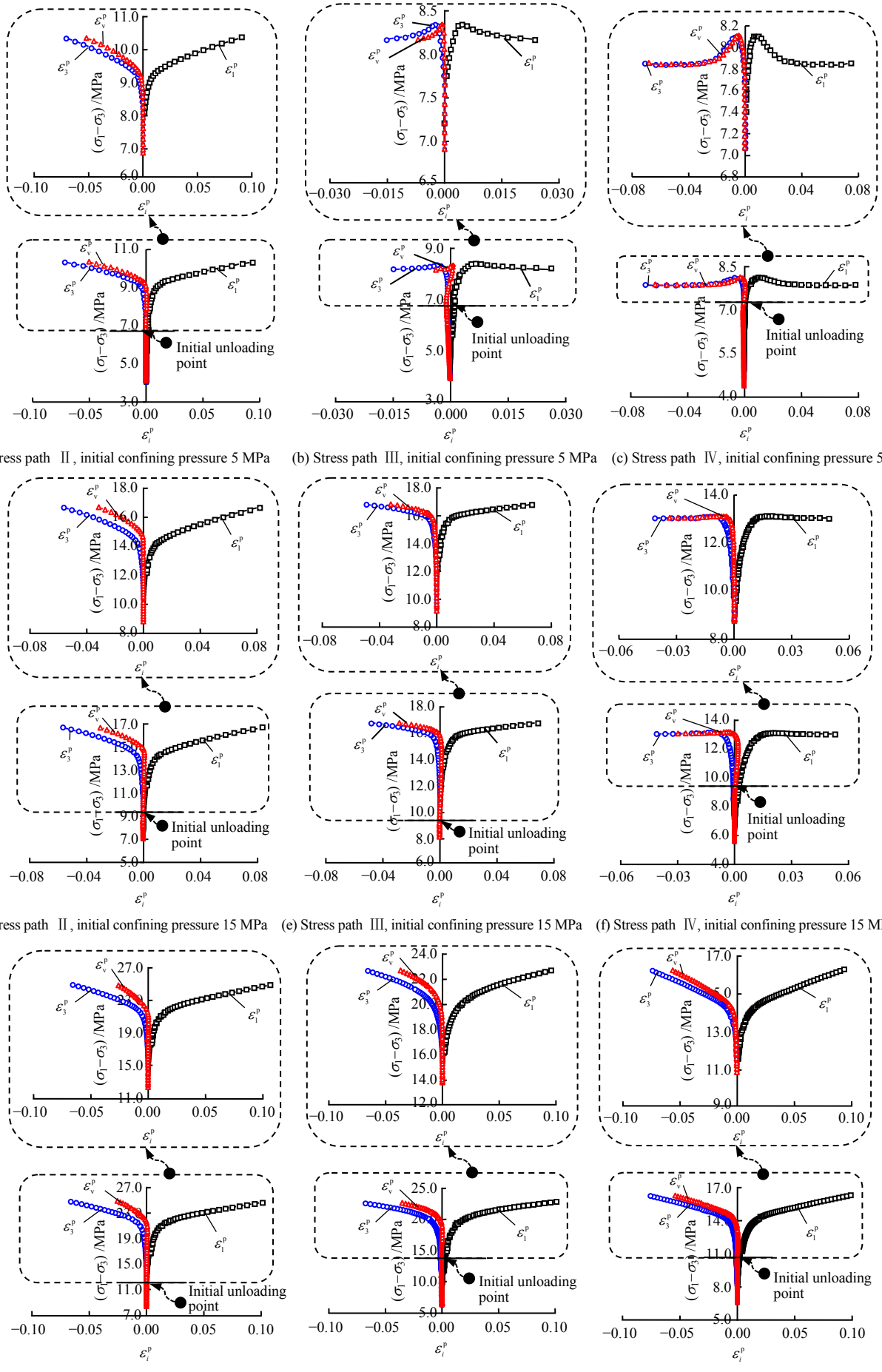

(a) Stress path Ⅱ, initial confining pressure 5 MPa (b) Stress path Ⅲ, initial confining pressure 5 MPa (c) Stress path Ⅳ, initial confining pressure 5 MPa

(d) Stress path Ⅱ, initial confining pressure 15 MPa (e) Stress path Ⅲ, initial confining pressure 15 MPa (f) Stress path Ⅳ, initial confining pressure 15 MPa

(g) Stress path Ⅱ, initial confining pressure 25 MPa (h) Stress path Ⅲ, initial confining pressure 25 MPa (i) Stress path Ⅳ, initial confining pressure 25 MPa

Fig. 8 Typical stress−plastic strain curves of samples from the staggered zone

was particularly important when determining the loading conditions. The basic property of stress path independence should be satisfied when selecting hardening parameters. On this basis, this article analyzed the variation differences of equivalent plastic work, equivalent plastic strain and plastic volumetric strain of staggered zone in the process from the same unloading starting point to unloading bearing limit and then to unloading stable loading limit (Fig. 5 (c)) under the complex unloading stress path, and explored whether it is feasible to take the above internal variables as the hardening parameters for staggered zone under the complex high in-situ stress unloading conditions.

The equivalent plastic work W^{p} is calculated by Eq. (7) [11],

$$W^{\mathrm{p}} = \int \mathrm{d}W^{\mathrm{p}} = \int \sigma_i \mathrm{d}\varepsilon_i^{\mathrm{p}} \tag{7}$$

Here,

$$\mathrm{d}W_1^{\mathrm{p}} = \sigma_1 \mathrm{d}\varepsilon_1^{\mathrm{p}} \tag{8}$$

$$\mathrm{d}W_3^{\mathrm{p}} = \sigma_3 \mathrm{d}\varepsilon_3^{\mathrm{p}} \tag{9}$$

$$\mathrm{d}W^{\mathrm{p}} = \mathrm{d}W_1^{\mathrm{p}} + 2\mathrm{d}W_3^{\mathrm{p}} \tag{10}$$

where W_1^{p} and W_3^{p} are the equivalent plastic work components in two principal stress directions; and $\varepsilon_1^{\mathrm{p}}$ and $\varepsilon_3^{\mathrm{p}}$ are the plastic strain components in two principal stress directions, respectively.

The equivalent plastic strain is calculated by the Eq. (11)[14]

$$\gamma^{\mathrm{p}} = \int \mathrm{d}\gamma^{\mathrm{p}} \tag{11}$$

Here,

$$\mathrm{d}\gamma^{\mathrm{p}} = \sqrt{(2/3)\mathrm{d}e_{ij}^{\mathrm{p}}\mathrm{d}e_{ij}^{\mathrm{p}}} = \sqrt{(4/3)J_2'} \tag{12}$$

where e_{ij}^{p} is the plastic deviant strain component; and J_2' is the second strain deviant invariant.

Equation (12) is further deduced and simplified:

$$\mathrm{d}\gamma^{\mathrm{p}} = \sqrt{-(2/3)\left(4\mathrm{d}e_1^{\mathrm{p}}\mathrm{d}e_3^{\mathrm{p}} + 2\mathrm{d}e_3^{\mathrm{p}}\mathrm{d}e_3^{\mathrm{p}}\right)} \tag{13}$$

$$e_1^{\mathrm{p}} = \varepsilon_1^{\mathrm{p}} - (\varepsilon_1^{\mathrm{p}} + 2\varepsilon_3^{\mathrm{p}})/3 \tag{14}$$

$$e_3^{\mathrm{p}} = \varepsilon_3^{\mathrm{p}} - (\varepsilon_1^{\mathrm{p}} + 2\varepsilon_3^{\mathrm{p}})/3 \tag{15}$$

where e_1^{p}, e_2^{p} and e_3^{p} are the plastic deviant strain components in three principal stress directions.

The equation for calculating plastic volumetric strain is listed by Eq. (16)[31],

$$\varepsilon_{\mathrm{v}}^{\mathrm{p}} = \varepsilon_1^{\mathrm{p}} + 2\varepsilon_3^{\mathrm{p}} \tag{16}$$

According to the calculation method of bearing capacity limit of unloading and bearing capacity limit of unloading stable loading adopted in Section 3.1, two bearing capacity limits of the triaxial test of the staggered zone under different confining pressures and different stress paths were calculated. As two loading yield surfaces, the influence differences of stress paths of the above internal variables were considered. It could be seen from Fig. 4 that all stress paths kept consistent before unloading under the same confining pressure. It was assumed that plastic deformation occurred at the beginning of unloading, namely, the initial unloading point was the initial yield surface, denoted as Ω_0. When the deviatoric stress reached to the capacity limit of unloading under the unloading stress path, it was regarded as the loading yield surface Ⅰ and denoted as Ω_{I}. When the deviatoric stress reached the bearing capacity limit of unloading stable loading under the unloading stress path, it was regarded as the loading yield surface Ⅱ and denoted as Ω_{II}. To compare the differences of different internal variables under different confining pressures and unloading stress paths, the internal variables were normalized without dimension.

In this section, the dimensionless normalization of equivalent plastic work from yield surface Ω_0 to loading surface Ω_{I} under initial confining pressure of 5 MPa was analyzed as an example. Firstly, the equivalent plastic work $W_{\mathrm{II}}^{\mathrm{p}}$, $W_{\mathrm{III}}^{\mathrm{p}}$ and $W_{\mathrm{IV}}^{\mathrm{p}}$ under three different unloading stress paths was calculated by Eq. (7). Then, the dimensionless normalized parameters of equivalent plastic work corresponding to each unloading stress path could be denoted as $\overline{W_{\mathrm{II}}^{\mathrm{p}}}$, $\overline{W_{\mathrm{III}}^{\mathrm{p}}}$ and $\overline{W_{\mathrm{IV}}^{\mathrm{p}}}$, respectively:

$$\overline{W_i^{\mathrm{p}}} = \frac{W_i^{\mathrm{p}}}{W_{\mathrm{II}}^{\mathrm{p}} + W_{\mathrm{III}}^{\mathrm{p}} + W_{\mathrm{IV}}^{\mathrm{p}}} \tag{17}$$

According to the calculation rule of the normalized internal variable, the internal variables were independent of the stress path when $\overline{W_{\mathrm{II}}^{\mathrm{p}}} = \overline{W_{\mathrm{III}}^{\mathrm{p}}} = \overline{W_{\mathrm{IV}}^{\mathrm{p}}} = 1/3$. They could therefore be used as the hardening parameters. However, they were believed to be closely related to the stress paths if the normalized internal variables under different stress paths differed greatly. Therefore, it was inappropriate to take them as hardening parameters.

The calculated normalized internal variables under different confining pressures and unloading stress paths were plotted into the same graph (see Fig. 9) for comparative analysis.

It could be seen from Fig. 9(a) that the equivalent plastic work was basically equal under low confining pressure (5 MPa) when the staggered zone changed from the yield surface Ω_0 to the loading surface Ω_{I} along different unloading stress paths, showing the independency of stress path. However, under high confining pressures (15 MPa, 25 MPa), the equivalent plastic work from the yield surface Ω_0 to the loading surface Ω_{I} along stress path Ⅳ (unloading axial pressure and unloading confining pressure) was slightly larger than that along stress path Ⅲ (constant axial pressure and unloading confining pressure) and

that along stress path Ⅱ (increasing axial pressure and unloading confining pressure). The equivalent plastic strain was independent of stress path only at high confining pressure (25 MPa). The equivalent plastic strain of the stress path Ⅳ from the yield surface Ω_0 to the loading surface Ω_{I} along different unloading stress paths under initial confining pressure of 5 MPa and 15 MPa was the maximal, that of the stress path Ⅲ was the middle, and that of the stress path Ⅱ was the minimal. The plastic volumetric strain showed the strong dependency of stress path under different confining pressures, and the change of the plastic volumetric strain under stress path Ⅳ was the most intense. In addition, the dependency of stress path of normalized internal variables in the process from the yield surface Ω_0 to the loading surface Ω_{II} along different unloading stress paths was described in Fig. 9(b). It could be seen that the changed law of internal variables was basically consistent with Fig. 9(a). And it showed that the above internal variables (the equivalent plastic work, the equivalent plastic strain, the plastic volumetric strain) varied from the initial yield surface to different loading surfaces in the same way. Therefore, the study of the independence of stress path of internal variables was independent of the selection of loading surface, as long as the staggered zone was guaranteed to reach the same loading surface from the same yield surface along different stress paths. Additionally, it could also be seen from Fig. 9 that the equivalent plastic work was more appropriate as the hardening parameter among the above internal variables, followed by the equivalent plastic strain, the plastic volumetric strain of the staggered zone was not suitable as the hardening parameter under the complicated unloading stress path.

4.2 Modification of hardening parameters of staggered zone under complex stress paths

According to study of the dependence of stress path of the equivalent plastic work, the equivalent plastic strain, the plastic volumetric strain and other internal variables as hardening parameters in Section 4.1, it could be seen that these internal variables all had a certain of the dependence of stress path. If they were directly used as the hardening parameter to describe the hardening law under the unloading stress path of the staggered zone, there will be a certain theoretical deviation when exploring its elastic-plastic constitutive relationship. But compared with plastic volumetric strain, the equivalent plastic work and the equivalent plastic strain could reduce the effect of stress path to some degree. Among them, the independency of stress path of the equivalent plastic work was the strongest. Therefore, it was considered to further modify the equivalent plastic work to better meet the definition of the independency of stress path of hardening parameters.

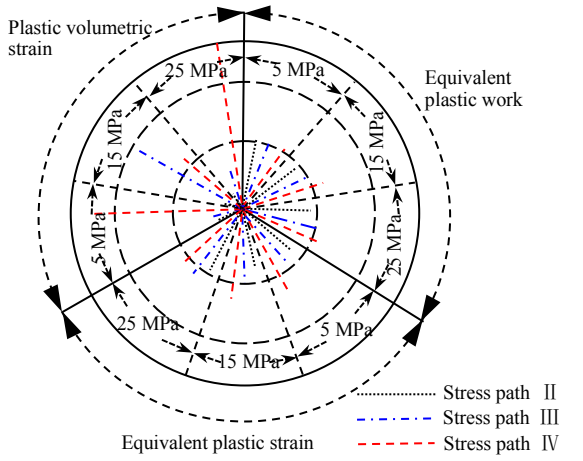

(a) Normalized internal variables from the yield surface Ω_0 to the loading surface Ω_{I} along different unloading stress paths

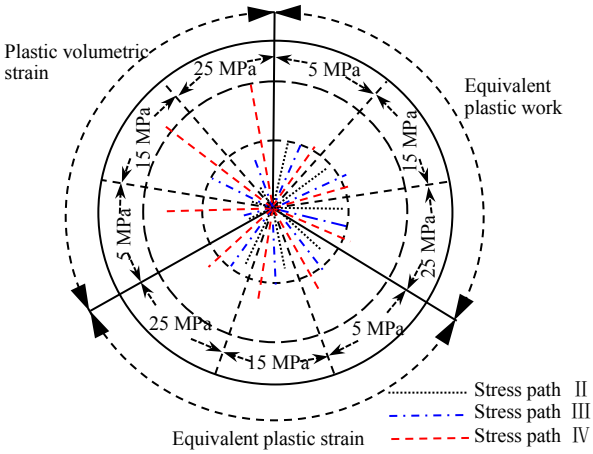

(b) Normalized internal variables from the yield surface Ω_0 to the loading surface Ω_{II} along different unloading stress paths

Fig. 9 The influence of stress path of normalized internal variables of staggered zone during the unloading process

To obtain hardening parameters accorded with the definition of hardening parameters, Moroto[21] proposed an energy-type parameter $W_{\mathrm{p}}^{\mathrm{m}}$ for the independency of stress path for granular materials:

$$W_{\mathrm{p}}^{\mathrm{m}}=\int\left[\left(t\mathrm{d}\varepsilon_{\mathrm{s}}^{\mathrm{p}}+s\mathrm{d}\varepsilon_{\mathrm{v}}^{\mathrm{p}}\right)\Big/\left(s/p_{\mathrm{a}}\right)\right] \tag{18}$$

where t is the maximum shear stress under bidirectional stress; s is the average principal stress under bidirectional stress; $\varepsilon_{\mathrm{s}}^{\mathrm{p}}$ is plastic shear strain; and p_{a} is one engineering atmospheric pressure (p_{a} =98.1 kPa).

Peng et al.[22] applied the above energy-type hardening parameters to the loading stress path of sand with the ratio of equal stress, and found that this parameter was better than the traditional plastic work, but there was still a certain of difference in the stress path. Therefore, a material parameter n related to the properties of granular materials was proposed (Eq. 19) to further modify the above energy-type hardening parameters [22]:

$$W_{\mathrm{p}}^{*}=\int\left[\left(t\mathrm{d}\varepsilon_{\mathrm{s}}^{\mathrm{p}}+s\mathrm{d}\varepsilon_{\mathrm{v}}^{\mathrm{p}}\right)\Big/\left(s/p_{\mathrm{a}}\right)^{n}\right] \tag{19}$$

where W_{p}^{*} is the modified plastic work; and n is the parameter related to the properties of granular materials.

When constructing the unified hardening function, Yao et al.[16−18] provided an idea for constructing hardening parameters, namely, founding a stress path-dependent factor R to remove components of the plastic volumetric strain increment $\mathrm{d}\varepsilon_{\mathrm{v}}^{\mathrm{p}}$ that are associated with the stress path, and then obtaining the hardening parameters with the independency of the stress path by integrating along the stress path. The unified hardening function was still independent of the loading path under complex loading path through verification [16−18].

Here, the aforesaid thought of constituting hardening parameters and the method of modifying the plastic work of energy-type parameters were adopted to propose the theoretical formula of the staggered zone for modifying the equivalent plastic work under the complex unloading stress path:

$$W^{\mathrm{p}+}=\int\left[\left(\sigma_1\mathrm{d}\varepsilon_1^{\mathrm{p}}+2\sigma_3\mathrm{d}\varepsilon_3^{\mathrm{p}}\right)\Big/T^{n_{\mathrm{s}}}\right] \tag{20}$$

$$T=\left[\left(\sigma_1+2\sigma_3\right)/\left(3p_{\mathrm{a}}\right)\right] \tag{21}$$

where $W^{\mathrm{p}+}$ is the modified equivalent plastic work; n_{s} is the parameter reflecting the properties of granular materials containing residual soft and rock debris; and T is the parameter related to the stress state. p_{a} is used to cancel out the dimension of T, making it be a dimensionless parameter.

By using revised Eqs. (20) and (21) of the equivalent plastic work, the parameter n_{s} (n_{s}= −0.4) representing the material properties of the staggered zone was obtained by continuous adjustments, and the modified equivalent plastic work of the staggered zone from the yield surface Ω_0 to the loading surface Ω_{I} along different unloading stress paths under different confining pressures was calculated and was normalized together with the equivalent plastic work in Section 4.1 without dimensionality so as to compare the stress path independency between them.

η is the standard deviation of normalized equivalent plastic work parameters of different stress paths, and a smaller value of η means a higher independency of stress of hardening parameters, namely:

$$\eta=\sqrt{\left(1/m\right)\sum_{i=1}^{m}\left(x_i-\bar{x}\right)^2}\ \left(i=1,2,3\right) \tag{22}$$

where x_1, x_2 and x_3 correspond to the normalized equivalent plastic work of stress paths Ⅱ, Ⅲ and Ⅳ, respectively; $\bar{x}$ is the average value of normalized equivalent plastic work ($\bar{x}=1/3$); and m is the number of different stress paths in the test (m=3).

The comparative analysis diagram of the dependency of stress path of equivalent plastic work before and after modification from the yield surface Ω_0 to the loading surface Ω_{I} along different unloading stress paths of the staggered zone under different confining pressures was plotted in Fig. 10. According to the definition of dimensionless normalized parameters of equivalent plastic work in Section 4.1, the closer equivalent plastic work was under the same confining pressure and different unloading stress paths (the shorter the error bar was, the smaller the standard deviation η was), the higher the independence of stress path was. Fig. 10(a) being taken as an example, the left of Fig. 10(a) was the equivalent plastic work before modification. The standard deviation of errors was obviously larger than the modified equivalent plastic work on the right, namely the modified equivalent plastic work as the hardening parameter of the staggered zone under high in-situ stress unloading condition had higher independency of stress path, and it was more suitable to describe the unloading hardening process of plastic strain. With the increase of initial confining pressure, the modified effect deteriorated to some degree. However, when the initial confining pressure increased to 25 MPa, the standard deviation of the modified equivalent plastic work η under different unloading stress paths was only 0.007 in this test, which suggested the modified equivalent plastic work of the staggered zone under different unloading stress paths also had high independency of stress path under high confining pressure (25 MPa). Therefore, the modified equivalent plastic work proposed in this paper met the assumption that hardening parameters had the independency of stress path in the elastic-plastic model construction theory of geotechnical plastic mechanics. Therefore, it was reasonable to use the modified equivalent plastic work proposed in this paper as the hardening parameter in the elastic-plastic analysis of the unloading process of high in-site stress staggered zone.

5 Engineering significance

5.1 Guiding significance of field failure mechanism and disaster prevention and control

From the engineering perspective, the rock mass from the staggered zone on the surface of the cavern after excavation was basically in a low confining pressure stress environment. The above different types of stress path tests of the unloading confining pressure could approximately simulate the mechanical behavior of the staggered zone in the field environment. Due to the difference in scale between the study of unloading mechanical properties in laboratory tests and the stagger zone of large underground caverns, the absolute values of plastic deformation parameters determined in laboratory tests cannot be directly applied to engineering, the regularity of plastic deformation revealed by the tests can however be generalized and help understanding of deformation and failure mechanism of rock masses in field staggered zone.

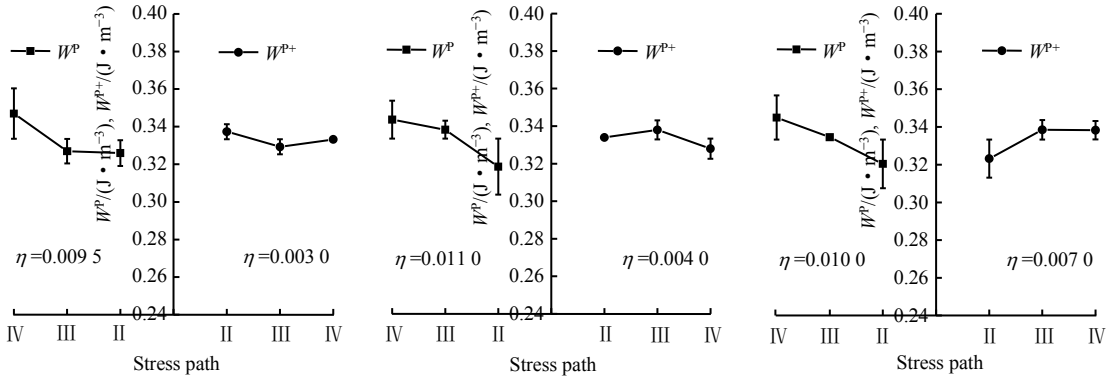

(a) Initial confining pressure 5 MPa (b) Initial confining pressure 15 MPa (c) Initial confining pressure 25 MPa

Fig. 10 Verification of the independency of stress path for modified equivalent plastic work

(1) When the staggered zone was exposed at the arch shoulder or foot of caverns, the strong unloading effect and the gravity effect would lead to the rapid decrease of the bonding strength of the staggered zone/parent rock interface, and the broken rock mass in the footwall of the staggered zone was difficult to stabilize itself, which would not only accompany with the local strong relaxation of the joint surface, but also even cause the continuous opening and sliding of the joint surface. This was consistent with the plastic deformation law revealed by the typical stress path Ⅱ or Ⅲ (the maximum principal stress σ_1 kept unchanged or increased while the minimum principal stress σ_3 decreased sharply) in the above tests. Namely, the axial compressive plastic strain and circumferential tensile plastic strain of the staggered zone increased sharply staring from unloading, and the rapid expansion and connection of cracks in rock mass from the staggered zone led to severe plastic deformation, coupled with the structure of broken rock mass from the staggered zone itself. Therefore, it was easy to collapse or fall block during the excavation with high in-situ stress unloading.

(2) When the staggered zone was exposed at the high side wall of a large underground cavern and the crossing caverns, the disturbances with excavation of multiple working faces led to the rock mass from the staggered zone in an unfavorable multi-face unloading stress environment, which corresponded to the plastic deformation law revealed by the experimental stress path Ⅳ (the maximum principal stress σ_1 and minimum principal stress σ_3 both decreased sharply). Namely, the plastic volumetric strain of the staggered zone increased dramatically, and the bearing capacity limit of unloading deteriorated the most, showing the strong dilatancy characteristics. Besides, the expansion of long-term plastic volumetric would made it gradually extrude to the surface of the plastic extrusion failure [3−7].

(3) On the premise of clarifying the harm of complex high in-situ stress unloading stress path in the staggered zone, the stress path of the staggered zone was experienced the excavation could be improved through the optimization design of excavation and support, to achieve the purpose of the failure prevention and control of rock mass from the staggered zone in the underground engineering.

5.2 Theoretical significance of modifying hardening parameters of staggered zone

In the plastic state, the stress-strain relationship of rock mass and soil was nonlinear and closely associated with stress path, stress history and loading and unloading states. The hardening parameter function of modified equivalent plastic work of the staggered zone under complex unloading stress path was constructed according to the relevant hardening parameter modification method and thought. And loading conditions with hardening parameters could be introduced to describe the phenomenon of the yield surface continuous expansion during the plastic deformation process, which improves the accuracy of the mechanical model in describing the plastic deformation stage and provides theoretical basis for modifying or establishing the reasonable mechanical model for the staggered zone under complex high in-situ stress unloading conditions.

Additionally, the constructed ideas and methods of hardening parameters of staggered zone were studied. For example, the characteristics of granular materials was characterized by the parameter n_s, and the reasonable modified equivalent plastic work could be found as the hardening parameter to describe its hardening characteristics. It also provided important reference for the determination of hardening parameters of other similar rocks and soil granular materials.

6 Conclusions

Based on a series of test results with triaxial unloading stress path of the staggered zone, combined with the geotechnical plastic mechanics theory, the plastic deformation law of the staggered zone under different unloading conditions was summarized, and the dependency of stress path of the equivalent plastic work, the equivalent plastic strain, the plastic volumetric

strain and other hardening parameters was analyzed. A general expression was proposed for modifying the hardening parameter of equivalent plastic work and some conclusions and understandings were obtained as follows:

(1) The plastic deformation of the staggered zone under high in-situ stress unloading conformed the following law. Under the same unloading stress path, the greater the confining pressure was, the greater the deviatoric stress was when the same circumferential plastic strain was produced. And the development of circumferential plastic strain was inhibited under high confining pressure. Under the same confining pressure, the promoting effect of different unloading stress paths on the plastic volumetric deformation of staggered zone was stress path Ⅳ ＞ stress path Ⅲ ＞stress path Ⅱ. But under the same circumferential plastic deformation, the deviatoric stress of the staggered zone in stress path Ⅳ was the lowest, followed by that in stress path Ⅲ, that in stress path Ⅱ was the highest.

(2) When the independency of stress path of internal variables was studied, the loading surface could be arbitrarily selected, but the staggered zone should be guaranteed to reach the same loading surface from the same yield surface along different stress paths. The equivalent plastic work was more suitable to be used as the hardening parameter of the staggered zone under complex unloading stress path than the equivalent plastic strain, and the plastic volumetric strain was not suitable to be used as the hardening parameter.

(3) To further reduce the dependency of stress path of equivalent plastic work, the equivalent plastic work was modified on the basis of existing research. It was found that the modified equivalent plastic work had higher independency of stress path when the parameter describing the material properties of the staggered zone, n_s equaled −0.4, which was more appropriate for describing the unloading plastic strain hardening characteristics of the staggered zone under high in-situ stress unloading conditions.

References

[1] PAN Jia-zheng. Hydropower and China[J]. Journal of Hydroelectric Engineering, 2004, 30(12): 17−21.

[2] XU Ding-ping, FEGN Xia-ting, CUI Yu-jun, et al. On failure mode and shear behavior of rock mass with interlayer staggered zone[J]. Rock and Soil Mechanics, 2012, 33(1): 129−136.

[3] DUAN Shu-qian, FENG Xia-ting, JIANG Quan, et al. Experimental study of mechanical properties of staggered zones under loading and unloading conditions of high stresses[J]. Chinese Journal of Rock Mechanics and Engineering, 2016, 35(6): 1090−1101.

[4] DUAN S Q, FENG X T, JIANG Q, et al. In situ observation of failure mechanisms controlled by rock masses with weak interlayer zones in large underground cavern excavations under high geostress[J]. Rock Mechanics and Rock Engineering, 2017, 50(9): 2465−2493.

[5] DUAN Shu-qian, FENG Xia-ting, JIANG Quan, et al. Mechanical characteristics of interlayer staggered zones under different preconsolidation pressures[J]. Rock and Soil Mechanics, 2017, 38(1): 49−60.

[6] DUAN S Q, JIANG Q, XU D P, et al. Experimental study of mechanical behavior of interlayer staggered zone under cyclic loading and unloading condition[J]. International Journal of Geomechanics, 2020, 20(3): 04019187-1-04019187-12.

[7] DUAN S Q, JIANG Q, LIU G F, et al. An Insight into the excavation-induced stress paths on mechanical response of weak interlayer zone in underground cavern under high geostress[J]. Rock Mechanics and Rock Engineering, 2021, 54(3): 1331−1354.

[8] WANG Jing-tao, ZHOU Bao-chun. Demonstration on dependency of constitutive relations of soils with stress paths[J]. Chinese Journal of Rock Mechanics and Engineering, 2008, 27(Suppl. 1): 2269−2674.

[9] CAI Y Q, HAO B B, GU C, et al. Effect of anisotropic consolidation stress paths on the undrained shear behavior of reconstituted Wenzhou clay[J]. Engineering Geology, 2018, 242: 22−33.

[10] LI Jian-peng, GAO Ling, MU Huan-sheng. Dilatancy characteristics of sandstone and its function of dilatancy angle under high confining pressure and unloading conditions[J]. Rock and Soil Mechanics, 2019, 40(6): 2119−2126.

[11] ZHENG Ying-ren, KONG Liang. Plastic mechanics of rock and soil[M]. Beijing: China Architecture & Building Press, 2010.

[12] JIANG Jia-qi, XU Ri-qing, YU Jian-lin, et al. An equivalent plastic work hardening model for clay based on the egg-shaped yield function[J]. Chinese Journal of Rock Mechanics and Engineering, 2021, 40(3): 619−628.

[13] FUMIO T. Stress-strain behavior of an idealized anisotropic granular material[J]. Soils and Foundations, 1980, 20(3): 75−90.

[14] HUANG Wen-xi. Theory of elastoplastic stress strain model for soil[J]. Rock and Soil Mechanics, 1979, 2(1): 1−20.

[15] HUANG Wen-xi, PU Jia-liu, CHEN Yu-jiong. Hardening rule and yield function for soils[J]. Chinese Journal of Geotechnical Engineering, 1981, 3(3): 19−26.

[16] YAO Yang-ping, HOU Wei, LUO Ting. Unified hardening model for soils[J]. Chinese Journal of Rock

Mechanics and Engineering, 2009, 28(10): 2135−2151.

[17] YAO Yang-ping, TIAN Yu, ZHOU An-nan, et al. Unified hardening law for soils and its construction[J]. Scientia Sinica (Technologica), 2019, 49(1): 26−34.

[18] YAO Y P, SUN D A, MATSUOKA H. A unified constitutive model for both clay and sand with hardening parameter independent on stress path[J]. Computers and Geotechnics, 2007, 35(2): 210−222.

[19] MA Xian-feng, MOCHIZUKI A, CAI Min. Development of elastoplastic model with revised plastic work function hardening function based on plane strain tests[J]. Chinese Journal of Geotechnical Engineering, 2007, 29(6): 887−893.

[20] MA Xian-feng, LIU Chang, XU Liang-yi. Application of modified double yield surface model in foundation excavation of soft soil[J]. Chinese Journal of Rock Mechanics and Engineering, 2019, 38(Suppl.2): 3883−3893.

[21] MOROTO N. Shearing deformation of granular materials such as sand[R]. Hachinohe: Department of Civil Engineering, Hachinohe Institute of Technology, 1980.

[22] PENG Fang-le, BAI Xiao-yu, YA Xin, et al. Modified plastic-work hardening parameter and function independent of stress path for sandy soil[J]. Chinese Journal of Rock Mechanics and Engineering, 2008, 27(6): 1171−1180.

[23] QIU Shi-li, FENG Xia-ting, ZHANG Chuan-qing, et al. Experimental research on mechanical properties of deep marble under different initial damage levels and unloading path[J]. Chinese Journal of Rock Mechanics and Engineering, 2012, 31(8): 1686−1697.

[24] WAN Zheng, QIU Ren-dong, SONG Chen-chen. A structural constitutive model of undisturbed saturated clays based on the uniform hardening parameter[J]. Chinese Journal of Rock Mechanics and Engineering, 2019, 38(9): 1905−1918.

[25] ZHAO Yang, ZHOU Hui, FENG Xia-ting, et al. Undrained shear behaviour of intact infilled joint soil with triaxial shear tests under high pressure and its influence factor analysis[J]. Rock and Soil Mechanics, 2013, 34(2): 365−371.

[26] Ministry of Water Resources of People's Republic of China. GB/T50123 — 1999 Standard for soil test method[S]. Beijing: China Planning Press, 1999.

[27] MENG Guo-tao, FAN Yi-lin, JIANG Ya-li, et al. Key rock mechanical problems and measures for huge caverns of Baihetan hydropower plant[J]. Chinese Journal of Rock Mechanics and Engineering, 2016, 35(12): 2549−2560.

[28] YANG Ai-wu, YANG Shao-kun, ZHANG Zhen-dong. Experimental study of mechanical properties of dredger fill under different unloading rates and stress paths[J]. Rock and Soil Mechanics, 2020, 41(9): 2891−2900.

[29] LIU Jie, ZHANG Li-ming, CONG Yu, et al. Research on the mechanical characteristics of granite failure process under true triaxial stress path[J]. Rock and Soil Mechanics, 2021, 42(8): 2069−2077.

[30] DENG Hua-feng, YUAN Xian-fan, LI Jian-lin, et al. Research on failure characteristics and determination method for compressive strength of soft rock in triaxial loading and unloading tests[J]. Rock and Soil Mechanics, 2014, 35(4): 959−964.

[31] DING Xiang, ZHANG Guang-qing WANG Zhi-ying. Coefficient of the effective plastic strain based on associated flow of Drucker-Prager criterion[J]. Chinese Journal of Applied Mechanics, 2017, 34(1): 1−7.